Numerical simulation and experimental validation of deposited corners of any angle in direct ink writing

Yongqiang Tu[a], Alaa Hassan[b,*], Ali Siadat[c], Gongliu Yang[d], Zhangwei Chen[a]

[a] Additive Manufacturing Institute, College of Mechatronics and Control Engineering, Shenzhen University, Shenzhen 518060, PR China

[b] ERPI, Université de Lorraine, F-54000 Nancy, France

[c] LCFC, Arts et Métiers ParisTech, F-57000 Metz, France

[d] School of Instrumentation and Optoelectronic Engineering, Beihang University, Beijing 100191, PR China

*Corresponding author: alaa.hassan@univ-lorraine.fr (A. Hassan)

Abstract

Direct ink writing (DIW) belongs to material extrusion based additive manufacturing (MEAM) and the molding quality of deposited corners has an impact on the geometrical quality of three dimensional (3D) parts fabricated by DIW. To fully understand the DIW process and improve the geometrical quality of parts, numerical simulations have been widely used to model the DIW process. However, the previous research works for numerical simulation of deposited corners could only achieve the corner simulation under the condition of small angle and failed to realize corner simulation of any angel. Herein, we propose an improved numerical simulation of deposited corners of any angle based on the use of volume of fluid (VOF) method and validate the proposed numerical simulation experimentally. For this purpose, the numerical simulation is conducted through geometrical modeling, meshes generation and boundary conditions determination. In the numerical simulation, deposited corner is realized by constructing two calculation areas where two nozzle velocities with the corner angle as the velocity direction angle are applied on the substrates of two calculation areas. The effectiveness of the proposed numerical model is validated through corners deposition experiments using a commercially available microcrystalline wax (MW)-based ink in a DIW 3D printer as simulated results fit experimental results well. The current work demonstrates an effective approach for the prediction of the deposited corners of any angle in DIW based on numerical simulations.

Keywords

Numerical simulation; Experimental validation; Deposited corners; Direct ink writing; Volume of fluid method

Statements and Declarations

Authors contributions

YT: Methodology, Simulation, Test, Writing–original draft. AH: Conceptualization, Writing–review & editing. AS: Supervision. GY: Supervision. CZ: Conceptualization, Writing–review & editing.

Funding

This work has been supported by the China Scholarship Council (No. 201906020135).

Data availability

The authors confirm that all data and materials reported in this paper are available.

Conflict of interest

On behalf of all authors, the corresponding author states that there is no conflict of interest.

Ethical approval

Not applicable.

Consent to participate

Not applicable.

Consent to publish

Not applicable.

Nomenclature			
α	Phase fraction	$\mathbf{n}$	Normal vector to ink surface
V_i	Volume of ink in a mesh	$\hat{\mathbf{n}}$	Unit vector normal to ink surface
V_m	Total volume of a mesh	$\hat{\mathbf{n}}_w$	Unit vector normal to wall
ρ_s	Density of single continuum	$\hat{\mathbf{t}}_w$	Unit vector tangent to wall
μ_s	Viscosity of single continuum	θ_c	Static contact angle
ρ	Density of ink	$\mathbf{U_r}$	Velocity vector compressing two-phase free surface
ρ_a	Density of air	c	Controllable compression factor
μ	Viscosity of ink	v_e	Average velocity in nozzle
μ_a	Viscosity of air	D_p	Piston diameter
$\dot{\gamma}$	Shear rate	D_n	Outer diameter of nozzle
μ_0	Limiting dynamic viscosity	d_n	Inner diameter of nozzle
τ_0	Yield stress	v_p	Piston velocity
K	Consistency index	L_n	Nozzle length
n	Flow index	h	Distance between nozzle bottom and substrate
$\mathbf{U}$	Velocity field	$\mathbf{v_{n1}}$	Nozzle velocity applied on substrate 1
p	Pressure	$\mathbf{v_{n2}}$	Nozzle velocity applied on substrate 2
$\mathbf{g}$	Gravitational acceleration vector	θ	Corner angle
$\mathbf{F_\sigma}$	Surface tension	v_{nx}	Nozzle velocity component along x axis
σ	Surface tension coefficient	v_{ny}	Nozzle velocity component along y axis
κ	Surface curvature		

1. Introduction

Direct ink writing (DIW) belongs to material extrusion based additive manufacturing (MEAM) and has become one of the most popular additive manufacturing (AM) techniques in the applications of rubber industry [1], tissue engineering [2], batteries [3], electronic circuits [4], ceramic engineering [5], sensors [6], 4D printing [7], food processing engineering [8] and buildings [9] due to its diversity in materials and flexibility in equipment [10]. During DIW, the feedstock is prepared as paste or slurry type material named ink and the ink has the shear-thinning rheological property and a good shape retention property [11-13]. Then the ink is filled in a syringe and extruded by a piston from a nozzle into a substrate layer by layer forming a three dimensional (3D) part [14].

The geometrical quality of 3D parts fabricated by DIW is influenced by the molding quality of

deposited corners [15]. Several scholars have done researches on improving the geometrical quality of MEAM by controlling quality of deposited corners [16-19]. Akhoundi et al. [16] improved the quality of corners through printing speed optimization to realize high-quality printed composites with different geometric shapes for MEAM. Giberti et al. [17] presented a path planning technology to maintain a constant velocity along the trajectory in corners aimed at improving dimensional quality for MEAM. Jin et al. [18] proposed an optimized path planning technique to decrease the number of sharp corners in MEAM to improve deposition quality of printed parts. Li et al. [19] improved precision of deposited corners and parts of MEAM by in-situ monitoring and predicting 3D geometric deviation.

In recent years, to fully understand the DIW process and improve the geometrical quality of parts in DIW, numerical simulation methods have been widely used to model the MEAM process [20-23]. Comminal et al. simulated the strand deposition [20] and the material deposition along a toolpath with a sharp corner [21] with computational fluid dynamics (CFD) models to study the effect of process parameters on deposited filaments and corners, respectively. Göhl et al. [22] conducted computer based simulations for DIW to evaluate newly developed inks. Tu et al. [23] established a model of freeform extruded filaments with numerical simulation and then evaluate the filaments based on the model for DIW. However, the previous work [21] for numerical simulation of deposited corners could only achieve the corner simulation under the condition of small angle which was less than 90° but failed to realize corner simulation of any angel. Thus, to overcome the limitation of the previous research for numerical simulation of deposited corners and fully realize DIW process modeling based on the application of numerical simulation, it is crucial and required to propose an improved numerical simulation to model deposited corners of any angle.

In this work, 3D numerical simulations of deposited corners of any angle in DIW are established with volume of fluid (VOF) method and corner deposition experiments are conducted using a commercially available Microcrystalline Wax (MW)-based ink to validate the proposed numerical simulation. The work overcomes the limitation of previous research works in numerical simulation of deposited corners and demonstrates an effective approach for prediction of deposited corns of any angle in DIW with computer based numerical simulation.

2. Volume of fluid method

The key of numerical simulation of deposited corners is to capture the interface between ink and air. Thus, the 3D numerical modeling for deposited corners is regarded as a two-phase flow simulation. For numerical simulation of two-phase flow problem, level set method [24], phase field method [25], lattice-Boltzmann method [26], direct interface tracking method [27] and volume of fluid (VOF) method [28] are most commonly used. Considering the advantages in simplicity, robustness and straightforward implementation [29], the VOF is selected as numerical simulation method for numerical simulations of deposited corners.

In VOF, the ink and air are treated as a single continuum and the phase fraction α is defined to distinguish the interface between the two-phase fluid as follows [30]:

$$\alpha = \frac{V_i}{V_m} \tag{1}$$

Where α is the phase fraction for a mesh; V_i is the volume of the ink in a mesh; V_m is the total volume of a mesh. α=0 when the mesh is filled with air and α=1 when the mesh is filled with ink. In the meshes along boundary between ink and air, the value of α belongs to (0,1). α=0.5 is defined as the cutoff value to capture the sharp front of interface between the ink and air.

Fluid properties of the single continuum are weighted with the phase fraction as follows:

$$\rho_s = \alpha\rho + (1-\alpha)\rho_a \tag{2}$$

$$\mu_s = \alpha\mu + (1-\alpha)\mu_a \tag{3}$$

Where ρ_s and μ_s is density and viscosity of the single continuum; ρ and ρ_a is density of the ink and air, respectively; μ and μ_a is viscosity of the ink and air, respectively.

μ is expressed using the Hershel-Bulkley due to its shear-thinning behavior as follows [31]:

$$\mu = \min\left(\mu_0, \tau_0 / \dot{\gamma} + K\dot{\gamma}^{n-1}\right) \tag{4}$$

Where $\dot{\gamma}$ is shear rate; μ_0, τ_0, K and n are rheological properties called as limiting dynamic viscosity, yield stress, consistency index, flow index for inks. μ_0, τ_0, K and n are determined through viscosity tests and data fitting of the experimental $\dot{\gamma}$ - μ data with Eq. (4).

The governing equations for the numerical simulation include continuity equation, momentum equilibrium equation and phase fraction equation. Each equation is written as follows [32]:

Continuity equation:

$$\nabla \cdot \mathbf{U} = 0 \tag{5}$$

Where $\mathbf{U}$ is velocity field of the fluid.

Momentum equilibrium equation:

$$\frac{\partial \rho_s \mathbf{U}}{\partial t} + \nabla \cdot \left(\rho_s \mathbf{U}\mathbf{U}\right) = -\nabla p + \nabla \cdot \left(\rho_s \mu_s \nabla \mathbf{U}\right) + \rho_s \mathbf{g} + \mathbf{F}_\sigma \tag{6}$$

Where p is the pressure in the fluid; $\mathbf{g}$ is the gravitational acceleration vector; $\mathbf{F}_\sigma$ is surface tension. $\mathbf{F}_\sigma$ is calculated as follows:

$$\mathbf{F}_\sigma = \sigma \kappa \nabla \alpha \tag{7}$$

where σ is the surface tension coefficient; κ is the surface curvature which is depended on the shape of deposited ink on the substrate. κ is computed from local gradients in the surface normal to the interface as follows [33]:

$$\kappa = \frac{1}{|\mathbf{n}|}\left(\left(\frac{\mathbf{n}}{|\mathbf{n}|} \cdot \nabla\right)|\mathbf{n}| - \nabla \cdot \mathbf{n}\right) \tag{8}$$

where $\mathbf{n} = \nabla \alpha$ is the normal vector to the ink surface. Wall adhesion between deposited ink and substrate is considered in the model based on the use of the static contact angle as:

$$\hat{\mathbf{n}} = \hat{\mathbf{n}}_w \cos\theta_c + \hat{\mathbf{t}}_w \sin\theta_c \tag{9}$$

where $\hat{\mathbf{n}} = \mathbf{n}/|\mathbf{n}|$ is the unit vector normal to the ink surface, $\hat{\mathbf{n}}_w$ and $\hat{\mathbf{t}}_w$ represents the unit vector normal and tangent to the substrate, respectively, θ_c is the static contact angle between the ink and substrate.

Phase fraction equation:

$$\frac{\partial \alpha}{\partial t} + \nabla \cdot \left(\alpha \mathbf{U}\right) + \nabla \cdot \left(\alpha\left(1-\alpha\right)\mathbf{U}_\mathbf{r}\right) = 0 \tag{10}$$

Where $\mathbf{U}_\mathbf{r}$ is velocity vector compressing two-phase free surface, which represents the velocity difference between two-phase fluids and can be calculated as follows:

$$\mathbf{U}_\mathbf{r} = \min\left(c|\mathbf{U}|, \max|\mathbf{U}|\right)\frac{\nabla \alpha}{|\nabla \alpha|} \tag{11}$$

Where c is controllable compression factor and it is selected as c=1 in the numerical simulation.

3. Numerical simulations

The free and open-source CFD software OpenFOAM v1912 [34] is used to realize the numerical simulation of the 3D profile of deposited corners as plotted in Fig. 1. In the numerical simulation, OpenFOAM v1912 is used to build geometrical model, generate meshes, determine boundary

conditions and solve governing equations. After numerical simulation in OpenFOAM v1912, ParaView, which is an open-source, multi-platform data analysis and visualization application [35], is used to build visualizations and analyze simulation data.

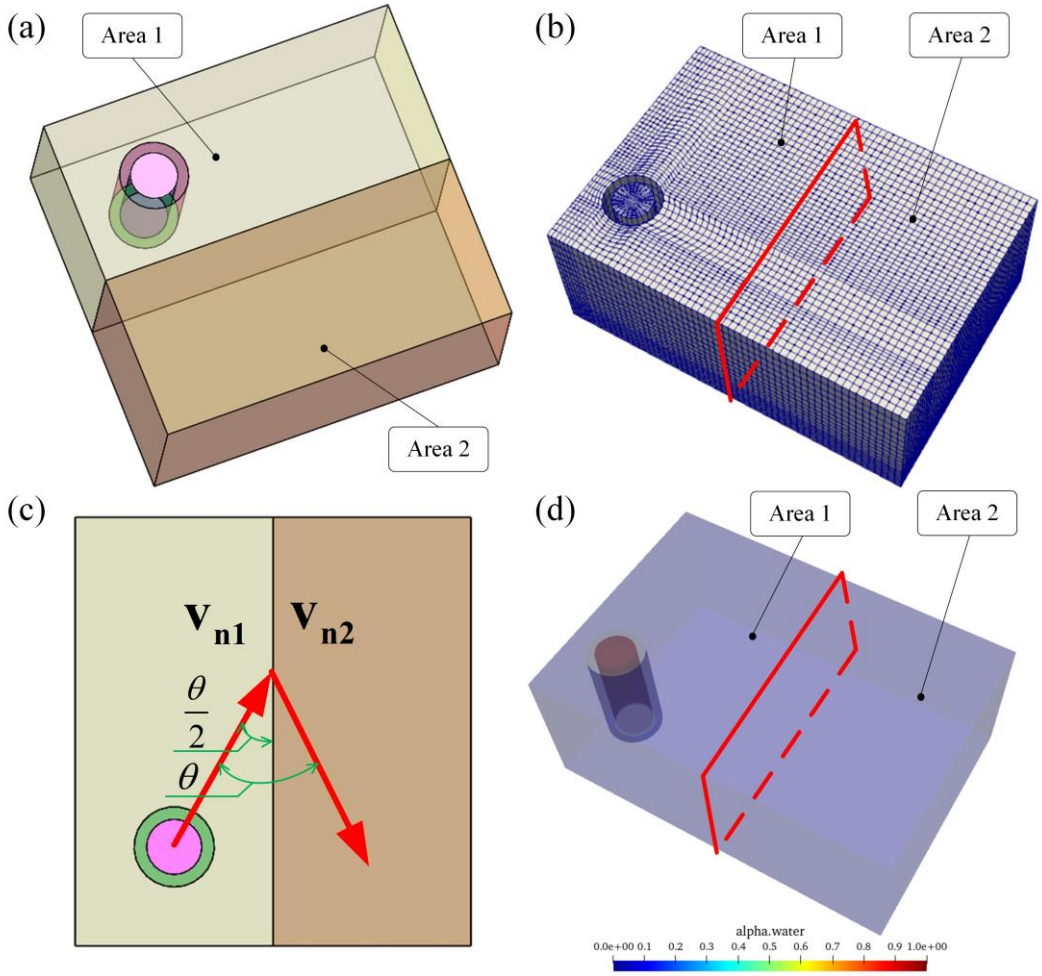

Fig. 1 Numerical modeling of 3D profile of deposited corners: (a) 3D geometrical model; (b) generated meshes; (c) velocity condition in substrates; (d) initial condition of phase fraction.

3.1. Geometrical model

The route of modeling of deposited corners of any angle in the proposed numerical simulation is to construct two computing areas, and simulate the corner of any angle by applying velocities of the same magnitude and different directions with the corner angle as the velocity direction angle to the substrates of the two computing areas. As shown in Fig. 1a, the geometrical model consists of two areas named as area 1 and area 2 where joint surface 1 in area 1 (Fig. 2a) and joint surface 2 in area 2 (Fig. 3a) are merged to combine area 1 and area 2 into a complete model. As shown in Fig. 2a, in area 1, the boundary surfaces include inlet, nozzle inner wall, nozzle outer wall, nozzle bottom wall, air, joint surface 1 and substrate 1. As illustrated in Fig. 2b, the critical parameters of area 1 include

the inner diameter of nozzle d_n, the outer diameter of nozzle D_n, the average velocity of ink in nozzle v_e, the nozzle length L_n, and the distance between nozzle bottom and substrate h. v_e is calculated using Eq. (12) based on the conservation of mass.

$$v_e = \left(D_p / d_n\right)^2 v_p \tag{12}$$

where v_p is the piston velocity and D_p is the piston diameter.

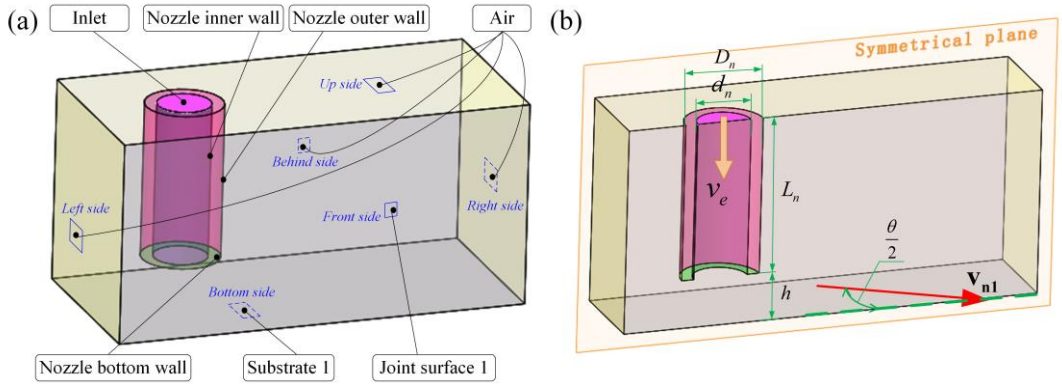

Fig. 2 Illustration of 3D geometrical model of area 1: (a) boundary surfaces; (b) critical parameters.

As shown in Fig. 3a, in area 2, the boundary surfaces include air, joint surface 2 and substrate 2. As illustrated in Fig. 3b, the critical parameters of area 2 include the h and the L_n. Area 2 is divided into area 201 and area 202 according to the values of L_n and h along the height direction as shown in Fig. 3b, where the area with the height of h from substrate 2 is area 202 and the rest is area 201

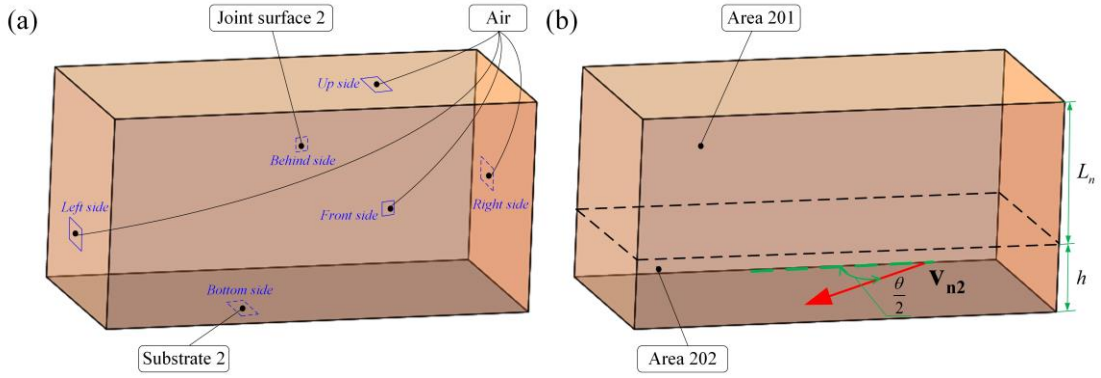

Fig. 3 Illustration of 3D geometrical model of area 2: (a) boundary surfaces; (b) critical parameters.

3.2. Generated meshes

As shown in Fig. 1b, meshes are generated as cuboid grids with arc edges in the areas related to circular nozzle and as cuboid grids with all straight edges in the areas outside the circular nozzle to

realize a smooth and precise interface simulation between ink and air. As illustrated in Fig. 4, to improve calculation efficiency and accuracy, meshes are refined in the region of deposited filaments including inner nozzle and area between nozzle bottom and substrate in area 1 (Fig. 4a) and area 201 in area 2 (Fig. 4b).

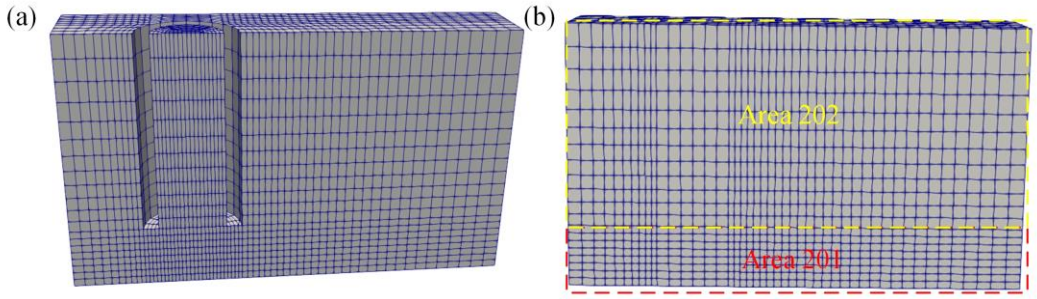

Fig. 4 Illustration of generated meshes in: (a) area 1; (b) area 2.

3.3. Boundary conditions

Velocity boundary conditions include the average velocity of ink in nozzle v_e on inlet, the nozzle velocity $\mathbf{v}_{n1}$ on substrate 1 and the nozzle velocity $\mathbf{v}_{n2}$ on substrate 2. v_e is calculated using Eq. (12). As illustrated in Fig. 1c, to avoid the model becoming a complex dynamic-mesh model which needs a large amount of computational time, the position of nozzle is fixed in the model while the substrate 1 is applied with a velocity $\mathbf{v}_{n1}$ and the substrate 2 is applied with a velocity $\mathbf{v}_{n2}$ in the boundary setting respectively as the movements of the nozzle and substrates are relative to each other. The values of $\mathbf{v}_{n1}$ and $\mathbf{v}_{n2}$ are same. The angel of $\mathbf{v}_{n1}$ and $\mathbf{v}_{n2}$ models the angle of deposited corners with the value of θ. The boundary conditions for the numerical simulation is summarized as in Table 1.

Table 1. Boundary conditions for the numerical simulation.

Name and physical meaning	Type	Setting
Inlet	Inlet	Velocity is set as v_e
Nozzle inner wall; nozzle outer wall; nozzle bottom wall	No-slip boundary	No-slip
Air	InletOutlet boundary	Depended on dynamic calculation
Substrate 1	No-slip boundary	Velocity is set as $\mathbf{v}_{n1}$
Substrate 2	No-slip boundary	Velocity is set as $\mathbf{v}_{n2}$

Fig. 1d presents the condition of phase fraction at the initial time which means the nozzle is filled with ink at the initial time, where red regime represents the ink and blue regime represents the air.

4. Experimental validation

4.1. Experimental setup

In order to validate the proposed numerical simulation, a commercially available MW-based ink, Nivea Crème Art. No. 80104 (Beiersdorf Global AG, Germany) is selected as ink reference as it is the printability reference and representative for ink preparation and process parameters selection for DIW [36]. As shown in Fig. 5, in the corner deposition experiments, the selected ink is filled into the syringe (Braun Melsungen AG, Germany) with a precision engineered fluid dispensing nozzle (Nordson EFD, USA), and then a piston driven DIW 3D printer TM-081 (Tobeca Company, France) is used to extrude ink in the syringe on the substrate forming deposited filaments and corners based on the design of G-code. After printing, a ruler is put aside the deposited corner, and a camera Logitech 720p (Logitech, Swiss) which is installed on the printer is used to take photos of deposited corners with the ruler. The photos are processed using the software Matlab to obtain the outline of deposited corners in real dimensions. In the image processing of experimental photos, the photo is transferred to grayscale and outline of deposited corner is obtained based on the use of canny edge detection; then outline in pixel coordinate is transferred into outline in real world coordinate by comparing the dimension of a pixel and the real dimension shown in ruler. Finally, the simulation results and experimental results of outlines in real world coordinate are compared in the software Matlab.

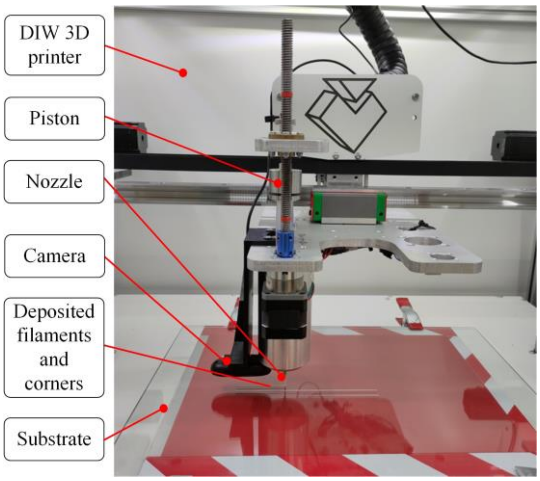

Fig. 5. Experimental validation setup for the numerical simulation.

4.2. Parameters setting in numerical simulations

Parameters in numerical simulations include parameters of material properties, critical parameters of geometrical model and process parameters. Parameters of material properties of the selected ink were obtained experimentally in our previous work [37] and are listed in Table 2. For critical parameters of geometrical model, the values of d_n, D_n and D_p are set as 0.84 mm, 1.22 mm, and 21.6 mm, which match the actual dimensions of the used DIW 3D printer in the experimental verification, respectively. As the nozzle length has no effect on v_e and the final deposited filaments and corners, the value of L_n is set as 2.44 mm which is smaller than practice nozzle length (18 mm) to reduce computational time.

Table 2 Paremeters of material properties of the commercially available MW-based ink Nivea Crème.

Parameter	Density ρ (kg/m^3)	Surface tension coefficient σ (mN/m)	Static contact angle θ_c (°)	Limiting dynamic viscosity μ_0 (Pa.s)	Yield stress τ_0 (Pa)	Consistency index K (Pa.s^n)	Flow index n
Value	972	43	180	1.58×10^6	563	867	0.045

Deposition status and the profile dimension of the deposited filaments are influenced by process parameters including v_e, h and the value of $\mathbf{v}_{n1}$ and $\mathbf{v}_{n2}$ [38, 39]. To select a suitable process parameters combination for a stable and regular deposited filament, θ is set as 0 and only area 1 is used in the numerical simulation to model deposited filaments without corners using different process parameters combinations in the printable window. Process parameters are selected as: v_e =6 mm/s; h =0.75 mm; the value of $\mathbf{v}_{n1}$ and $\mathbf{v}_{n2}$ is 4.8 mm/s; because deposited filaments under this process parameters combination has a stable and regular 3D shape and cross-sectional profile as shown in Fig. 6. Finally, to model deposited corners of any angle, the value of θ is set from 30° to 150° with the interval of 30° in numerical simulations and experiments to validate the numerical simulation of deposited corners of any angle.

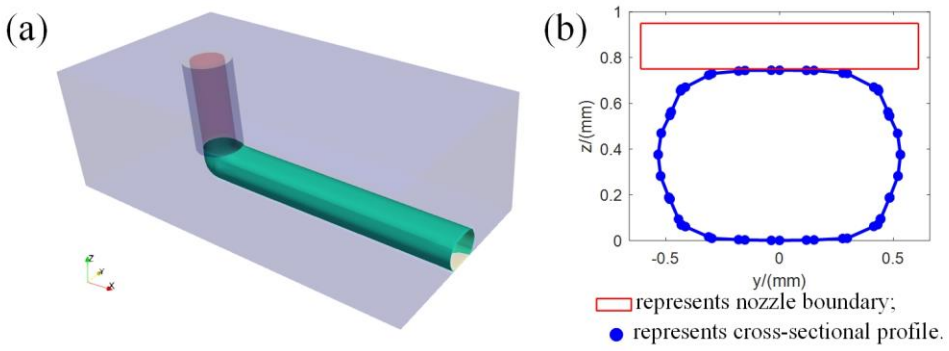

Fig. 6. Simulated deposited filaments under the selected process parameters combination: (a) 3D profile; (b) cross-sectional profile.

5. Results and discussion

Fig. 7 represents the 3D profile and top view of simulated deposited corners and top view of experimental results for deposited corners where the value of θ is set from 30° to 150° with the interval of 30°. Comparison of simulation and experimental results is conducted in the software Matlab using image processing and plotted in Fig. 8.

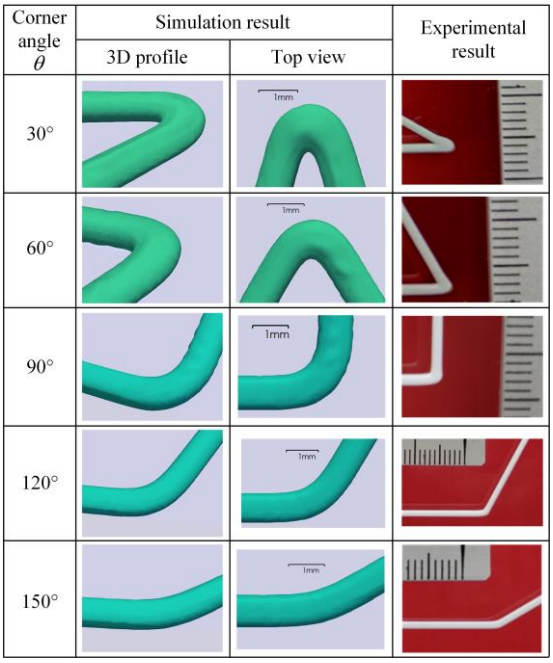

Fig. 7. Simulation and experimental results of deposited corners.

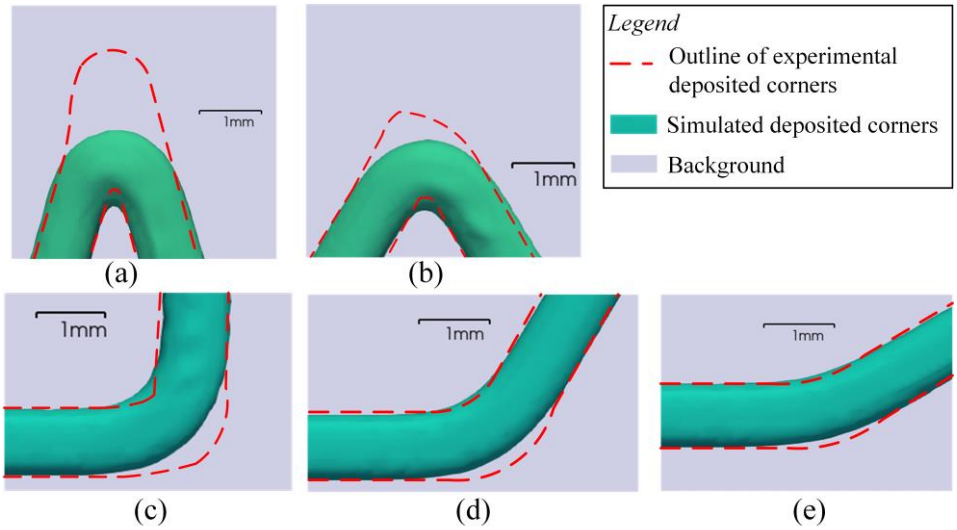

Fig. 8. Comparison of simulation and experimental results of deposited corners when θ is set as: (a) 30°; (b) 60°; (c) 90°; (d) 120°; (e) 150°.

As shown in Fig. 8, the deposited filaments and corners of any angle in numerical simulations fit outlines of experimental results well in outline of deposited filament and corner angle. Thus, the proposed numerical simulation is validated as an effective method to model deposited corners of any angle. However, the accuracy of the simulation with respect to the theoretical profile of the corners is lower than that in the filaments. The reason for this phenomenon is due to the difference between the nozzle velocity applied on substrate in numerical simulation and real nozzle velocity in experiments only for the corner region. As shown in Fig. 9a, the trajectory of nozzle velocity applied on substrate is from point A to point B and then from point B to point C. As illustrated in Fig. 9b and Fig. 9c, in numerical simulation, the value of velocity on substrate along x axis is a constant v_{nx} along the trajectory, and the value of velocity on substrate along y axis can change from v_{ny} to $-v_{ny}$ at point B immediately. In practice experiments, the nozzle cannot change

velocity immediately and need a uniform deceleration and uniform acceleration process to change nozzle velocity direction [40] and the acceleration depends on the firmware of the DIW 3D printer [21]. As shown in Fig. 10a, the trajectory of nozzle velocity applied on substrate is divided into 4 stages as follows where detail velocity profile along x axis and y axis is plotted in Fig. 10b and Fig. 10c, respectively:

- Point A to point B_1: uniform velocity process;
- Point B_1 to point B_2: uniform deceleration process;
- Point B_2 to point B_3: uniform deceleration process;
- Point B_3 to point C: uniform velocity process.

Comparing Fig. 9 and Fig. 10, the difference of nozzle velocity between numerical simulation and real experiment leads to the simulation error in corner regions. As shown in Fig. 8, the simulation error decreases as the corner angle increases which means that the effect of difference of nozzle velocity between numerical simulation and real experiment on deposited corners decreases as the corner angle increases.

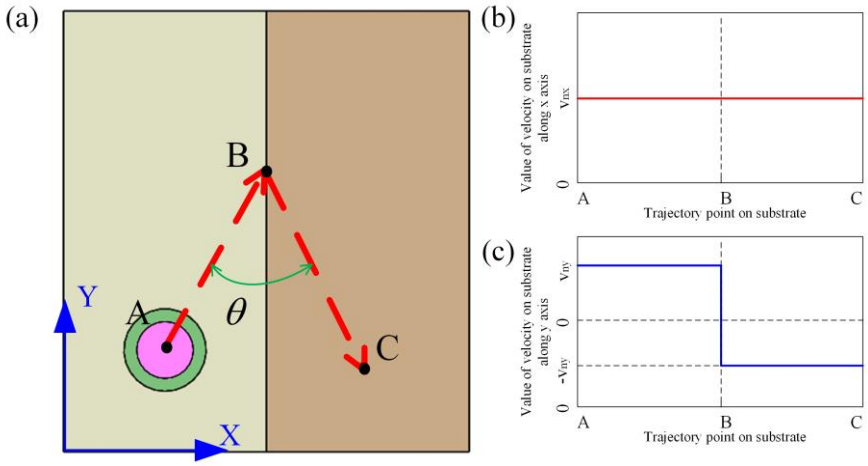

Fig. 9. Velocity profile on substrate in numerical simulation and design of G-code: (a) trajectory; (b) value of velocity on substrate along x axis; (c) value of velocity on substrate along y axis.

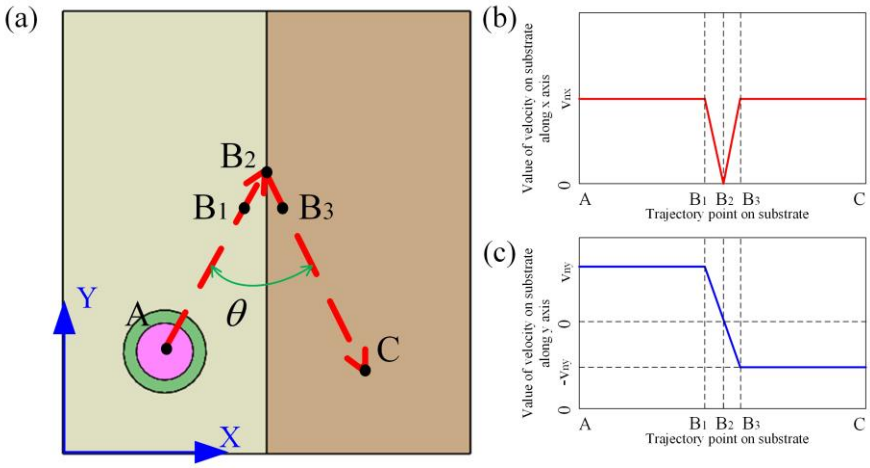

Fig. 10. Velocity profile on substrate in actual corner deposition experiments: (a) trajectory; (b) value of velocity on substrate along x axis; (c) value of velocity on substrate along y axis.

6. Conclusion

The previous research works for numerical simulation of deposited corners could only achieve the corner simulation under the condition of small angle and failed to realize corner simulation of any angel. In this study, an improved 3D numerical simulation of deposited corners is established by using VOF method and by considering the overall ink material properties. The improved 3D numerical simulation overcomes the limitation of the previous work and realizes deposited corner modeling of any angle by constructing two calculation areas where two nozzle velocities with the corner angle as the velocity direction angle are applied on the substrates of two calculation areas. The effectiveness of the proposed numerical model is validated through corners deposition experiments using a commercially available MW-based ink in a DIW 3D printer as simulated results are consistent with experimental results well in outline of deposited filament and corner angle. It is observed that the simulation accuracy in corners is inferior than that in filaments. The reason for this phenomenon is due to the difference between the nozzle velocity applied on substrate in numerical simulation and real nozzle velocity in experiments only for the corner region as the nozzle needs a uniform deceleration and uniform acceleration process to change nozzle velocity direction in practice printing. The simulation error in the corner decreases as the corner angle increases. The present study suggests an effective numerical simulation for the deposition corners of any angle in DIW. It also provides a viable basis for the future work on the elaboration of numerical modeling of the overall DIW 3D printing process.

Future work could improve the proposed numerical simulation of deposited corners of any angle considering the practice velocity change process in real experiments to improve the simulation accuracy in corner region. And numerical simulations of printed layers and 3D parts could then be established based on the proposed numerical simulation of deposited corners of any angle.

References

[1] M. Kim, J.-W. Choi, Rubber ink formulations with high solid content for direct-ink write process, Additive Manufacturing 44 (2021) 102023.

[2] D.F.D. Campos, M.A. Philip, S. Gürzing, C. Melcher, Y.Y. Lin, J. Schöneberg, A. Blaeser, B. Theek, H. Fischer, M. Betsch, Synchronized Dual Bioprinting of Bioinks and Biomaterial Inks as a Translational Strategy for Cartilage Tissue Engineering, 3D Printing and Additive Manufacturing 6(2) (2019) 63-71.

[3] C. Liu, Y. Qiu, Y. Liu, K. Xu, N. Zhao, C. Lao, J. Shen, Z. Chen, Novel 3D grid porous Li4Ti5O12 thick electrodes fabricated by 3D printing for high performance lithium-ion batteries, Journal of Advanced Ceramics 11(2) (2022) 295-307.
[4] T. Kim, C. Bao, M. Hausmann, G. Siqueira, T. Zimmermann, W.S. Kim, 3D Printed Disposable Wireless Ion Sensors with Biocompatible Cellulose Composites, Advanced Electronic Materials 5(2) (2019) 1800778.
[5] Z. Ye, C. Chu, D. Zhang, S. Ma, J. Guo, Y. Cheng, G. Xu, Z. Li, A. Sun, Study on 3D-Direct Ink Writing based on adding silica submicron-particles to improve the rheological properties of alumina ceramic ink, Materials Today Communications 28 (2021) 102534.
[6] A. Kalkal, S. Kumar, P. Kumar, R. Pradhan, M. Willander, G. Packirisamy, S. Kumar, B.D. Malhotra, Recent advances in 3D printing technologies for wearable (bio)sensors, Additive Manufacturing 46 (2021) 102088.
[7] M.C. Mulakkal, R.S. Trask, V.P. Ting, A.M. Seddon, Responsive cellulose-hydrogel composite ink for 4D printing, Materials & Design 160 (2018) 108-118.
[8] M. Lille, A. Nurmela, E. Nordlund, S. Metsä-Kortelainen, N. Sozer, Applicability of protein and fiber-rich food materials in extrusion-based 3D printing, Journal of Food Engineering 220 (2018) 20-27.
[9] L.A. Vergara, H.A. Colorado, Additive manufacturing of Portland cement pastes with additions of kaolin, superplastificant and calcium carbonate, Construction and Building Materials 248 (2020) 118669.
[10] S. Tarassoli, Z. Jessop, A. Al-Sabah, I. Simoes, I. Whitaker, Searching for the optimal bioink in extrusion-based 3D bioprinting for reconstructive surgery, International Journal of Surgery 55 (2018) S95.
[11] S.A. Wilson, L.M. Cross, C.W. Peak, A.K. Gaharwar, Shear-Thinning and Thermo-Reversible Nanoengineered Inks for 3D Bioprinting, ACS Applied Materials & Interfaces 9(50) (2017) 43449-43458.
[12] J.L. Dávila, M.A. d'Ávila, Rheological evaluation of Laponite/alginate inks for 3D extrusion-based printing, The International Journal of Advanced Manufacturing Technology 101(1) (2019) 675-686.
[13] Z.M. Jessop, A. Al-Sabah, N. Gao, S. Kyle, B. Thomas, N. Badiei, K. Hawkins, I.S. Whitaker, Printability of pulp derived crystal, fibril and blend nanocellulose-alginate bioinks for extrusion 3D bioprinting, Biofabrication 11(4) (2019) 045006.
[14] Y. Jiang, X. Wang, J. Plog, A.L. Yarin, Y. Pan, Electrowetting-assisted direct ink writing for low-viscosity liquids, Journal of Manufacturing Processes 69 (2021) 173-180.
[15] T.J. Fleck, J.C.S. McCaw, S.F. Son, I.E. Gunduz, J.F. Rhoads, Characterizing the vibration-assisted printing of high viscosity clay material, Additive Manufacturing 47 (2021) 102256.
[16] B. Akhoundi, M. Nabipour, O. Kordi, F. Hajami, Calculating printing speed in order to correctly print PLA/continuous glass fiber composites via fused filament fabrication 3D printer, Journal of Thermoplastic Composite Materials (2021) 0892705721997534.
[17] H. Giberti, L. Sbaglia, M. Urgo, A path planning algorithm for industrial processes under velocity constraints with an application to additive manufacturing, Journal of Manufacturing Systems 43 (2017) 160-167.
[18] Y. Jin, J. Du, Z. Ma, A. Liu, Y. He, An optimization approach for path planning of high-quality and uniform additive manufacturing, The International Journal of Advanced Manufacturing

Technology 92(1) (2017) 651-662.
[19] L. Li, R. McGuan, R. Isaac, P. Kavehpour, R. Candler, Improving precision of material extrusion 3D printing by in-situ monitoring & predicting 3D geometric deviation using conditional adversarial networks, Additive Manufacturing 38 (2021) 101695.
[20] R. Comminal, M.P. Serdeczny, D.B. Pedersen, J. Spangenberg, Numerical modeling of the strand deposition flow in extrusion-based additive manufacturing, Additive Manufacturing 20 (2018) 68-76.
[21] R. Comminal, M.P. Serdeczny, D.B. Pedersen, J. Spangenberg, Motion planning and numerical simulation of material deposition at corners in extrusion additive manufacturing, Additive Manufacturing 29 (2019) 100753.
[22] J. Göhl, K. Markstedt, A. Mark, K. Håkansson, P. Gatenholm, F. Edelvik, Simulations of 3D bioprinting: predicting bioprintability of nanofibrillar inks, Biofabrication 10(3) (2018) 034105.
[23] Y. Tu, A. Hassan, J.A. Arrieta-Escobar, U.K.u. Zaman, A. Siadat, G. Yang, Modeling and evaluation of freeform extruded filament based on numerical simulation method for direct ink writing, The International Journal of Advanced Manufacturing Technology 120(5) (2022) 3821-3829.
[24] M.R. Hashemi, P.B. Ryzhakov, R. Rossi, An enriched finite element/level-set method for simulating two-phase incompressible fluid flows with surface tension, Computer Methods in Applied Mechanics and Engineering 370 (2020) 113277.
[25] J. Yang, J. Kim, A phase-field method for two-phase fluid flow in arbitrary domains, Computers & Mathematics with Applications 79(6) (2020) 1857-1874.
[26] L. Zheng, S. Zheng, Q. Zhai, Reduction-consistent axisymmetric lattice Boltzmann equation method for N-phase fluids, Computers & Fluids 218 (2021) 104857.
[27] M. Li, I.A. Bolotnov, The evaporation and condensation model with interface tracking, International Journal of Heat and Mass Transfer 150 (2020) 119256.
[28] N. Scapin, P. Costa, L. Brandt, A volume-of-fluid method for interface-resolved simulations of phase-changing two-fluid flows, Journal of Computational Physics 407 (2020) 109251.
[29] R. Comminal, W.R. Leal da Silva, T.J. Andersen, H. Stang, J. Spangenberg, Modelling of 3D concrete printing based on computational fluid dynamics, Cement and Concrete Research 138 (2020) 106256.
[30] J. Lian, X. Yang, B. Ma, W. Gou, A novel method for bounding the phase fractions at both ends in Eulerian multi-fluid model, Computers & Fluids 243 (2022) 105512.
[31] M.H. Kim, Y. Lee, W.-K. Jung, J. Oh, S.Y. Nam, Enhanced rheological behaviors of alginate hydrogels with carrageenan for extrusion-based bioprinting, Journal of the Mechanical Behavior of Biomedical Materials 98 (2019) 187-194.
[32] M.R.P. de Sousa, H.S. Santana, O.P. Taranto, Modeling and simulation using OpenFOAM of biodiesel synthesis in structured microreactor, International Journal of Multiphase Flow 132 (2020) 103435.
[33] A. Ashish Saha, S.K. Mitra, Effect of dynamic contact angle in a volume of fluid (VOF) model for a microfluidic capillary flow, Journal of Colloid and Interface Science 339(2) (2009) 461-480.
[34] C. Busse, I. Tsivilskiy, J. Hildebrand, J.P. Bergmann, Numerical modeling of an inductively coupled plasma torch using OpenFOAM, Computers & Fluids 216 (2021) 104807.
[35] Q. Liu, J. Li, J. Liu, ParaView visualization of Abaqus output on the mechanical deformation of complex microstructures, Computers & Geosciences 99 (2017) 135-144.

[36] N. Paxton, W. Smolan, T. Böck, F. Melchels, J. Groll, T. Jungst, Proposal to assess printability of bioinks for extrusion-based bioprinting and evaluation of rheological properties governing bioprintability, Biofabrication 9(4) (2017) 044107.
[37] Y. Tu, J.A. Arrieta-Escobar, A. Hassan, U.K.u. Zaman, A. Siadat, G. Yang, Optimizing Process Parameters of Direct Ink Writing for Dimensional Accuracy of Printed Layers, 3D Printing and Additive Manufacturing (2021).
[38] H. Yuk, X. Zhao, A New 3D Printing Strategy by Harnessing Deformation, Instability, and Fracture of Viscoelastic Inks, Advanced Materials 30(6) (2018) 1704028.
[39] M. Athanasiadis, A. Pak, D. Afanasenkau, I.R. Minev, Direct Writing of Elastic Fibers with Optical, Electrical, and Microfluidic Functionality, Advanced Materials Technologies 4(7) (2019) 1800659.
[40] D.S. Ertay, A. Yuen, Y. Altintas, Synchronized material deposition rate control with path velocity on fused filament fabrication machines, Additive Manufacturing 19 (2018) 205-213.